Article

# Application of the 4D Fingerprint Method with a Robust Scoring Function for Scaffold-Hopping and Drug Repurposing Strategies

Adel Hamza,[†,‡] Jonathan M. Wagner,[†,‡,#] Ning-Ning Wei,[○] Stefan Kwiatkowski,[†,§] Chang-Guo Zhan,[∥,⊥,§] David S. Watt,[†,§] and Konstantin V. Korotkov*,[†,‡]

[†]Department of Molecular and Cellular Biochemistry, [‡]Center for Structural Biology, [§]Center for Pharmaceutical Research and Innovation, College of Pharmacy, [∥]Molecular Modeling and Biopharmaceutical Center, and [⊥]Department of Pharmaceutical Sciences, College of Pharmacy, University of Kentucky, Lexington, Kentucky 40536, United States
[○]School of Life Science and Medicine, Dalian University of Technology, Panjin, LN 124221, China

Ⓢ *Supporting Information*
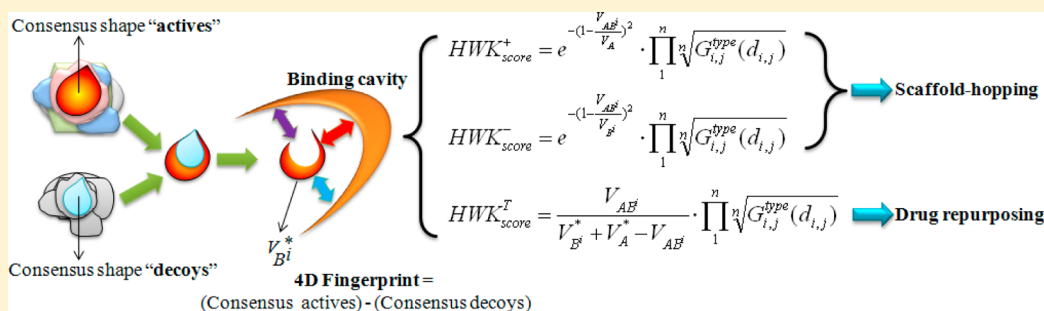
ABSTRACT: Two factors contribute to the inefficiency associated with screening pharmaceutical library collections as a means of identifying new drugs: [1] the limited success of virtual screening (VS) methods in identifying new scaffolds; [2] the limited accuracy of computational methods in predicting off-target effects. We recently introduced a 3D shape-based similarity algorithm of the SABRE program, which encodes a consensus molecular shape pattern of a set of active ligands into a 4D fingerprint descriptor. Here, we report a mathematical model for shape similarity comparisons and ligand database filtering using this 4D fingerprint method and benchmarked the scoring function *HWK* (Hamza–Wei–Korotkov), using the 81 targets of the DEKOIS database. Subsequently, we applied our combined 4D fingerprint and *HWK* scoring function VS approach in scaffold-hopping and drug repurposing using the National Cancer Institute (NCI) and Food and Drug Administration (FDA) databases, and we identified new inhibitors with different scaffolds of $MycP_1$ protease from the mycobacterial ESX-1 secretion system. Experimental evaluation of nine compounds from the NCI database and three from the FDA database displayed IC_{50} values ranging from 70 to 100 μM against $MycP_1$ and possessed high structural diversity, which provides departure points for further structure–activity relationship (SAR) optimization. In addition, this study demonstrates that the combination of our 4D fingerprint algorithm and the *HWK* scoring function may provide a means for identifying repurposed drugs for the treatment of infectious diseases and may be used in the drug-target profile strategy.

■ INTRODUCTION

Computational methodologies utilized for in silico high throughput screening (HTS) are a critical component of drug discovery approaches.[1−7] Within the available in silico HTS approaches, methodologies that combine ligand- and structure-based screening procedures find the widest application.[1,8] The challenge in any HTS virtual screening (VS) platform is to develop an algorithm that is sufficiently fast and robust to evaluate many compounds while maintaining sufficient accuracy to identify a subset of biological active compounds (i.e., hits) that have diverse structural scaffolds (i.e., scaffold-hopping). We sought to employ in silico screening to evaluate the repurposing of current drugs for a new therapeutic target.[9−11] Drug-repurposing maximizes the potential value of each hit by screening well-known compounds that have minimal toxicity and/or few side-effects.[12−14]

Comparative studies of well-established ligand- and docking-based approaches concluded that shape-based ligand screening yielded markedly better outcomes than protein docking schemes.[15−18] A ligand-based computational method involved two essential elements: [1] an efficient similarity measure and [2] a reliable scoring method. The similarity measure varied among different methods and focused on three factors: pharmacophores, molecular shapes, and molecular fields. The molecular-shape approaches maximized the overlap of shapes and determined a similarity value based on the degree of shape overlap. Over the years, despite the investment made in developing scoring functions for molecular-shape approaches, none possessed accuracy and general applicability. Every
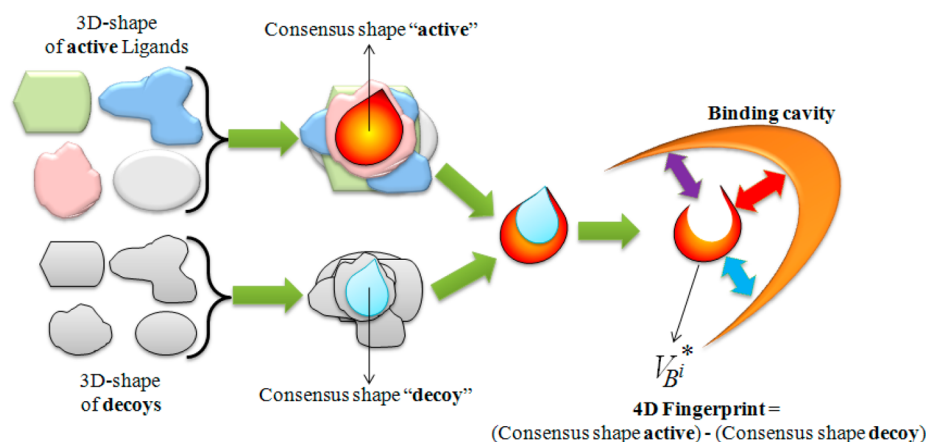
Figure 1. Ligand and structure shape-based VS approach using the 4D fingerprint. The resulting 4D fingerprint encoded in the 3D shape of the candidate ligand B^i is docked and ranked using the *HWK* scoring function. The application of the 4D fingerprint to the ligand B^i decreases the interaction (purple arrow) with the receptor.

scoring function had its advantages as well as its limitations. Consequently, investigators turned to the consensus-scoring technique that improved the probability of finding solutions by combining the scores from multiple scoring functions or using different reference molecules.[15,19−22]

We recently developed an efficient 3D shape-based similarity algorithm encoding the consensus molecular shape pattern of a set of active ligands into one descriptor, called the 4D fingerprint (Figure 1). The 4D fingerprint formalism was originally proposed by Hopfinger and co-workers and developed the quantitative structure−activity relationships (4D-QSAR) model.[23] The 4D-QSAR model estimates molecular similarity measures as a function of conformation, alignment, and atom type.[24] The resulting descriptors values were the occupancy measures for the atoms in the investigated set of bioactive molecules. While the similarity measures achieved excellent predictions for a variety of enzyme inhibitors,[25−27] the weakness of this approach lies with the occupancy measures for the atoms (or pharmacophoric groups) which may also be present in similar, "inactive" compounds.[28]

The 4D fingerprint approach implemented in the *Shape-Approach-Based Routines Enhanced* or SABRE program possessed a number of attractive advantages over other VS methods.[29,30] First, it depended explicitly on 3D shape, not on the underlying chemical structure, and thus it excelled in identifying novel chemical scaffolds based on a set of known active ligands (scaffold-hopping). The iterative 4D fingerprint approach was particularly robust for several reasons: (i) the 4D fingerprint descriptors were very sensitive to the details of molecular shape of active ligands, reducing the need to use multiple conformers of multiple query structures; (ii) the method excel by the incorporation of the spatial distributions of chemical features of similar inactive ligands during the optimization and screening procedures; (iii) the algorithm was fast and had the ability to scan a library of millions of compounds in a matter of hours. The method unified ligand- and structure-based 4D fingerprint VS approaches by docking the shape filtered ligand structures into the receptor-binding cavity. Finally, running searches using this methodology was remarkably easy and required only that the end-user supply a query structure and runtime parameters to control the number of hits that were returned. Despite these advantages, the 4D fingerprint method, as previously reported, suffered from a weakness in the empirical *HWZ* scoring function[17] for ranking

and selecting the active ligands from large databases. To remedy this deficiency, we modified the shape-based VS algorithm of the SABRE program and implemented a new, robust scoring function that accommodated the diversity of ligand scaffolds with an accuracy that exceeded our prior efforts.

Tuberculosis (TB) is a chronic and complex disease resulting from infection with the bacterium *Mycobacterium tuberculosis*. TB remains an important public health problem worldwide, with 8.6 million estimated cases and 1.3 million deaths attributed to the disease in 2012.[31] In order to combat the spread of TB—particularly resistant strains of *M. tuberculosis*—it is necessary to identify new molecular targets for TB drugs and develop new, more efficient, methods for screening ligands as potential drug candidates than methods used in the past. Historically, high-throughput screening (HTS) approaches coupled with in vitro testing served to identify promising hits with anti-TB activity. While successful in some cases, the HTS approach frequently failed in the antibacterial drug discovery area due to the poor ADMET properties and insufficient or improper molecular diversity of the compounds screened.[32,33] The mycobacterial ESX secretion system, also referred to as the type VII secretion system, represents a promising, new target for TB drug development.[34,35] The ESX secretion system is a specialized system unique to mycobacteria that secrete a large number of proteins necessary for *M. tuberculosis* virulence.[36−38] Each ESX secretion system includes a membrane-associated subtilisin-like protease, called the mycosin: $MycP_1$−$MycP_5$ (numbered according to gene cluster). $MycP_1$ from the ESX-1 system hydrolyzes the ESX associated protein B (EspB) during secretion,[39−41] and this processing affects virulence in a mouse model of TB infection.[42] The recent description of the molecular structure and substrate specificity of $MycP_1$[43−45] prompted interest in $MycP_1$ as a promising target for structure-based drug design.

Recently, we applied the combined ligand- and structure-based virtual screening procedure and 4D fingerprint algorithm to identify new inhibitors for $MycP_1$ protease.[30] The study reported here extends our previous work and reports a rational approach for ranking the ligand databases and demonstrates the performance of the novel *HWK* scoring function using 81 targets from the DEKOIS database.[46] Validation of the efficiency of the VS method for scaffold-hopping and drug repurposing involved the application of this methodology for the identification of diverse inhibitor scaffolds against $MycP_1$

protease and experimental testing of some of these scaffolds in an in vitro enzyme assay.

METHODS

We have recently developed a ligand and structure shape-based VS algorithm implemented within the SABRE program.[29,30] Unlike other ligand-based shape overlapping methods,[47−49] our approach efficiently detected the key pharmacophore groups of the active ligands responsible for binding to the target. The main advance of our methodology resided in the consideration of "virtual" but similar inactive structures (decoys) during the consensus molecular-shape detection process (Figure 1). After similarity scoring, the selected structures were ranked according to their shape complementarity in the receptor-binding site. This report highlights the major steps of the algorithm and describes the approach used for the development of this scoring function.

Enhanced Molecular Shape-Density Model. The molecular shape density function $\varphi(r)$ of a ligand is expressed in terms of the shape density functions of individual atoms and their overlap

$$\phi(\mathbf{r}) = 1 - \prod_i [1 - \rho_i(\mathbf{r})] \tag{1}$$

in which each atom i with coordinates $\mathbf{R}_i = (X_i, Y_i, Z_i)$ is described by a spherical Gaussian:[50−53]

$$\rho_i(\mathbf{r}) = p e^{-\left(\frac{3p\pi^{1/2}}{4\sigma_i^3}\right)^{2/3}(\mathbf{r}-\mathbf{R}_i)^2} \tag{2}$$

where σ_i is the van der Waals radius of the atom i. The molecular volume V of the ligand is defined as[54]

$$V = \int \phi(\mathbf{r})\, d\mathbf{r} = \sum_i v_i - \sum_{i<j} v_{ij} + \sum_{i<j<k} v_{ijk} - \sum_{i<j<k<l} v_{ijkl} + \dots \tag{3}$$

The volume v_i of an atom i is

$$v_i = \frac{4\pi\sigma_i^3}{3} \tag{4}$$

The intersection volume of atom pairs is defined as

$$v_{ij} = \int v_i(r) v_j(r)\, dr \tag{5}$$

The overlap volume of two molecules A and B is defined as

$$V_{AB} = \langle V_A | V_B \rangle = \int \varphi_A(r) \varphi_B(r)\, dr \tag{6}$$

In the SABRE algorithm, the shape-density model is enhanced and defined as a linear combination of weighted atomic Gaussian functions.[18,29,30] Thus, the molecular shape-density is the sum of all individual weighted pharmacophore densities, and the molecular volume is defined as

$$\begin{aligned} V &= \sum_k C_k V_k^{\text{pharm}-k} \\ &= c_1 V_1^{\text{pharm}-1} + c_2 V_2^{\text{pharm}-2} + c_3 V_3^{\text{pharm}-3} + \dots \\ &= V^{\text{PHARM}} + V_\varepsilon \end{aligned} \tag{7}$$

where $V_k^{\text{pharm}-k} = \sum_i \int d\mathbf{r}\, \rho_{ki}(\mathbf{r})$ is the partial volume of the pharmacophore group k and is defined as a linear combination of atomic Gaussian functions. The optimal coefficients $\{C_k\}$ are

determined by iteratively adjusting the coefficients of the set of known active ligands $\{A^i\}$ in the presence of virtual decoy structures $\{B^i\}$ (virtual decoys are inactive similar compounds that are not necessarily synthetically feasible or identified in the previous VS rounds) until they satisfy these two criteria:

$$A \in \{A^i\};\ \langle V_A | V_B \rangle$$
$$= \begin{cases} \text{max and } V^{\text{PHARM}} >> V_\varepsilon & \text{if } B \in \{A^i\} \\ \text{min and } V^{\text{PHARM}} << V_\varepsilon & \text{if } B \notin \{A^i\} \end{cases} \tag{7a}$$

This algorithm quickly builds a consensus molecular-shape pattern in which the optimal coefficients $\{C_k\}$ define a 4D fingerprint of the entire set of active ligands that also effectively excludes structurally similar, but inactive ligands (decoys) (Figure 1).[29,30]

Rational Approach for Developing a Robust and Efficient Scoring Function. Given a set of known active ligands $\{A_i\}$ with volumes $V_{\{Ai\}}$ and a query structure A with the volume V_A, we effect the shape-filtering and ranking the candidate molecule B^i with volume $V_B{}^i$.

During the VS process, we observe two trends: (i) $V_{Bi} \leq V_A$ or (ii) $V_{Bi} \geq V_A$. As a result, we can rank the structure B^i according to either the condition (i), (ii), or the combination of (i) and (ii) for two different ligands B^i and B^j. Thus, we have two possible outcomes:

(1) The volume of the candidate structure B^i is smaller than the volume of the query A: $V_{Bi} \leq V_A$. The maximal overlap volume V_{ABi} for the two structures is restricted as $V_{ABi} \leq V_{Bi}$ and rewritten as

$$0 \leq 1 - \frac{V_{AB^i}}{V_{B^i}} \tag{8}$$

(2) The volume of the structure B^i is larger than the volume of the query A: $V_{Bi} \geq V_A$ and $V_{ABi} \leq V_A$ is rewritten as

$$0 \leq 1 - \frac{V_{AB^i}}{V_A} \tag{9}$$

(3) We illustrate this case by considering two candidate structures with $V_{Bi} \leq V_A$ and $V_{Bj} \geq V_A$. For clarity we consider that they have the same overlap volume with the query structure and consequently, $V_{ABi} \approx V_{ABj}$. Adding eqs 8 and 9 gives

$$2V_{AB^i} \leq V_{B^i} + V_A \Rightarrow V_{AB^i} \leq V_{B^i} + V_A - V_{AB^i}$$

and we obtain the *Tanimoto* scoring function:[55]

$$\text{Tanimoto} = \frac{V_{AB^i}}{V_{B^i} + V_A - V_{AB^i}} \leq 1 \tag{10}$$

We rewrote eqs 8 and 9 as smooth Gaussian distributions and defined the scoring function *HWK* (Hamza−Wei−Korotkov) that converges to one for optimal similarity:

$$\text{If } V_{B^i} \leq V_A \qquad HWK^- = e^{-\left(1 - \frac{V_{AB^i}}{V_{B^i}}\right)^2} \tag{11}$$

$$\text{If } V_{B^i} \geq V_A \qquad HWK^+ = e^{-\left(1 - \frac{V_{AB^i}}{V_A}\right)^2} \tag{12}$$

The Tanimoto function and eqs 11 and 12 clearly reveal that the ranking of the candidate structure B^i is determined by

several inhomogeneous criteria. For a fixed overlap volume, eq 11 gives the highest score for the ligand B^i with a smallest size even if it possess less similar chemical features than other ligands with larger volume sizes. Second, the V_{ABi} term takes into account the overlap volume of the full ligand size instead the volume of the key chemical features present in both the query A, and candidate ligand B^i. This result in a higher ranking for the ligand B^i with largest size since the overlap volume varies with the full size of the ligand. Third, we recently demonstrated the weakness of the Tanimoto scoring function when used for filtering the 3D shape of the ligands and found that the Tanimoto function only efficiently ranks the ligands with comparable volume size to the query.[17]

These drawbacks can be overcome by taking into account the specific atom-type information, such as the consensus molecular shape pattern or "4D fingerprint" of the set of known active ligands. According to the 4D fingerprint approach (eq 7), the volume of the query A and the set of active ligands $\{A_i\}$ are defined as

$$V_A^* = V_A^{\text{PHARM}} + V_\varepsilon \quad \text{and} \quad V_{\{A^i\}}^* = V_{\{A^i\}}^{\text{PHARM}} + V_{\varepsilon'}^i \quad (13)$$

The optimization of the coefficients $\{c_k\}$ leads to the residual volume $V_\varepsilon \ll V_A^{\text{PHARM}}$, and the value of the V_A^{PHARM} term in eq 7 ranges across the interval $[\min V_{\{A^i\}}^{\text{PHARM}}; \max V_{\{A^i\}}^{\text{PHARM}}]$.

In the following demonstration, we assumed that the candidate B^i is an active ligand and similar to the query A in the set of active ligands $\{A_i\}$, since if B^i is dissimilar the overlap volume converges to a small value. We have

$$A \in \{A^i\} \quad \text{and} \quad B^i \in \{A^i\}$$

Using the computed 4D fingerprint coefficients, the volume of B^i is written as

$$V_{B^i}^* = V_{B^i}^{\text{PHARM}} + V_{\varepsilon''}^i \quad \text{with}$$
$$V_{B^i}^{\text{PHARM}} \in [\min V_{\{A^i\}}^{\text{PHARM}}; \max V_{\{A^i\}}^{\text{PHARM}}] \quad \text{or as}$$
$$V_{B^i}^* \in [\min(V_{\{A^i\}}^*); \max(V_{\{A^i\}}^*)] \quad (14)$$

the volume of B^{i*} is defined by eq 7 and is equals to the sum of the weighted partial volumes of the key pharmacophore groups and its volume size is in the interval of the set of active ligand volumes $V_{\{A^i\}}^*$.

Three possible scenarios exist:

(1) $V_{B^i}^* \leq V_A^*$
In this case, $V_{B^i}^* \in [\min(V_{\{A^i\}}^*); V_A^*]$ and the optimal similarity value is reached for

$$\max(V_{AB^i}) \approx V_{B^i}^* \Rightarrow HWK_{\text{score}}^- = e^{-\left(1 - \frac{V_{AB^i}}{V_{B^i}^*}\right)^2} \rightarrow e^{-\left(1 - \frac{V_{B^i}^*}{V_{B^i}^*}\right)^2}$$
$$\rightarrow 1$$

(2) $V_{B^i}^* \geq V_A^*$
In this case, $V_{B^i}^* \in [V_A^*; \max(V_{\{A^i\}}^*)]$ and the optimal similarity is reached for

$$\max(V_{AB^i}) \approx V_A^* \Rightarrow HWK_{\text{score}}^+ = e^{-\left(1 - \frac{V_{AB^i}}{V_A^*}\right)^2} \rightarrow 1$$

(3) According to the eqs 13 and 14 and the 4D fingerprint coefficients, the Tanimoto scoring function is written as $T = V_{AB^i}/(V_{B^i}^* + V_A^* - V_{AB^i})$ with

$$V_{B^i}^* \leq V_A^* \quad \text{then} \max(V_{AB^i}) \approx V_{B^i}^* \quad \text{and}$$
$$V_{B^j}^* \geq V_A^* \quad \text{then} \max(V_{AB^j}) \approx V_A^*$$

The optimal similarity is reached for $T^i = V_{B^i}^*/V_A^* \approx T^j = V_A^*/V_{B^j}^* \rightarrow 1$.

As a result, the candidate ligands with a volume size slightly smaller or larger than the query volume are ranked equivalently when using the 4D fingerprint method with the Tanimoto equation. Finally, we observe that the weighting coefficients of the 4D fingerprint adjust and group the unknown "*active*" candidate structures with miscellaneous volume sizes and scaffolds into three classes relative to the query size. This confers the advantage of ranking more effectively these three types of shape using the HWK scoring function (HWK^-, HWK^+, HWK^{Tanimoto}).

Shape-Fitting Procedure. The docking approach described in our previous work combined the performance and speed of the ligand-based 4D fingerprint method with the shape characteristic of the receptor binding site.[29] The current SABRE docking algorithm encodes both the 4D fingerprint and the novel HWK scoring function, and it generates alignments where patterns with similar binding character are oriented in a similar fashion in the binding site of the receptor (Figure 1). During the rigid docking process, the SABRE program takes into account only the pharmacophore groups present in the $V_{B^i}^{\text{PHARM}}(V_{B^i}^*)$ that interact in designated ways with key receptor atoms. Five important chemical features were assigned to an atom type: hydrogen bond donor, hydrogen bond acceptor, acidic center (negatively charged at physiological pH 7), basic center (positively charged at pH 7), and metal-chelation. The main novelty of the SABRE docking approach is that the pairwise interaction between the key pharmacophoric groups (defined by the 4D fingerprint, Figure 1) of the ligand and the receptor atoms are calculated using the Gaussian function G_{ij}. The pairwise interaction of atoms i (ligand atoms) and j (receptor atoms) is defined as

$$G_{i,j}^{\text{type}}(d_{i,j}) = 1 + \lambda^{\text{type}}\exp(-\omega^{\text{type}}(D_{\text{Eq}}^{\text{type}} - d_{i,j})^2) \quad (15)$$

where $D_{\text{Eq}}^{\text{type}}$ is the standard distance between the heavy atoms i and j for each "type" of interaction (i.e., hydrogen bond interaction, electrostatic interactions) and d_{ij} is the distance between the two atom centers. The parameter ω^{type} is a freely adjustable parameter and controls the distribution of the Gaussian function. The parameter λ^{type} controls the weight of the interaction type and depends on the 4D fingerprint coefficients.

The pairwise interaction is attractive for $\lambda^{\text{type}} > 0$ and repulsive for $\lambda^{\text{type}} < 0$. The total of n pairwise interactions between the pharmacophoric groups of the ligand and the key receptor atoms is defined by the geometric mean $G_{i,j}^{\text{TOTAL}}(d_{i,j})$ as

$$G_{i,j}^{\text{TOTAL}}(d_{i,j}) = (\prod_1^n G_{i,j}^{\text{type}}(d_{i,j}))^{1/n} = \prod_1^n \sqrt[n]{G_{i,j}^{\text{type}}(d_{i,j})}$$
$$(16)$$

Thus, the combination of the total pairwise interactions $G_{i,j}^{\text{TOTAL}}(d_{ij})$ and eqs 10−12 takes into account both the 4D fingerprint and the key interacting pharmacophoric groups of the ligand and leads to improved enrichment of the VS process. The HWK_{Dock} scoring function of the SABRE docking method is summarized by the three equations:

$$HWK_{Dock}^{-} = e^{-\left(1 - \frac{V_{AB^i}}{V_{B^i}}\right)^2} \cdot \prod_{1}^{n} \sqrt[n]{G_{i,j}^{type}(d_{i,j})} \tag{17}$$

$$HWK_{Dock}^{+} = e^{-\left(1 - \frac{V_{AB^i}}{V_{A}}\right)^2} \cdot \prod_{1}^{n} \sqrt[n]{G_{i,j}^{type}(d_{i,j})} \tag{18}$$

$$HWK_{Dock}^{Tanimoto} = \frac{V_{AB^i}}{V_{B^i}^* + V_{A}^* - V_{AB^i}} \cdot \prod_{1}^{n} \sqrt[n]{G_{i,j}^{type}(d_{i,j})} \tag{19}$$

It is interesting to note that a ligand with high similarity score (eqs 10−12) is reranked with a lower score if its chemical features are close to repulsive receptor atoms. Therefore, our scoring strategy developed in the docking method combines the fast and efficient ligand-shape-based 4D fingerprint VS with an extremely quick calculation of the interactions between the ligand pharmacophoric groups and the key receptor atoms. In addition, we observe in Figure 1 that the interaction (purple arrow) involving the pharmacophore groups present in both active and decoy structures become negligible. Analysis of the HWK_{Dock} function (eqs 17−19) highlights a new strategy for improving scaffold-hopping and drug repurposing perform-ances. During the VS campaign, the shape size of the query is fundamental and orients the choice of the scoring equations. Thus, if the shape of the query is small and does not completely fill the receptor binding cavity, the HWK_{Dock}^{+} is appropriate to identify structural hits with either comparable or larger volume sizes than the query volume. However, the hits with volume sizes ranging in the interval $[min(V_{\{A^i\}}^*); V_A^*]$ of the set of active ligands (eq 14) are also ranked with a high HWK_{Dock}^{+} score. In contrast, if the shape of the query complement the receptor binding cavity, the HWK_{Dock}^{-} is better suited to identify hits with smaller volume sizes while keeping high overlap volume with the pharmacophore groups of the query. Finally, the $HWK_{Dock}^{Tanimoto}$ is effective to identify hits with comparable query shape (i.e., rather smaller or larger structural sizes that fit into the receptor binding cavity while retaining structural diversity). Consequently, three different classes of hits emerge based on the equations of the HWK function that selected them. In each list, the compounds are first ranked according to query similarity using the 4D fingerprint approach, and the diversity is achieved by selecting compounds ranked highly using one of these scoring equations.

Evaluation of VS Efficiency and Robustness Using the Novel *HWK* Scoring Function. The DEKOIS (version 2.0) database of annotated active compounds and decoys was used to validate the *HWK* scoring function.[46] The DEKOIS database is a publicly available VS test database consisting of 81 targets. For our purposes, the ratio of the number of decoys to the number of active ligands was fixed at 30. We used the DEKOIS database instead of the 40 targets of the DUD database for our VS test in order to measure the robustness of the scoring function when screening a large number of targets. This is one of the most commonly encountered measures for estimating prediction accuracy of VS algorithms.

The effectiveness of the SABRE program was evaluated using the enrichment factor (EF) metric at a given percentage of the database screened,[56−58] and the area under the ROC (receiver operator characteristics). To test the efficiency of the *HWK* scoring function defined by eqs 10−12, we screened each target 10 times using a different set of five randomly selected active ligands (as templates) and reported both the highest perform-

ance (ROC AUC value) and enrichment factor *EF* at 1% for the 81 targets. Screening results using the empirical *HWZ* scoring function were reported for comparison.[17] For each screening test, the five template structures where first removed from the list of active ligands.

Identification of Potential Inhibitors of MycP$_1$ Protease. The detailed VS procedure was described in our previous work[30] and summarized in the Supporting Informa-tion (Supplementary Figure SI-1). Briefly, the 4D fingerprint algorithm defined in the 3D-shape-based similarity method of SABRE was used as the first filter of the NCI (National Cancer Institute) from the NCI Open Database Compounds (Release 4, ~265 000 structures) and FDA (Food and Drug Administration, 1217 compounds) database downloaded from the ZINC database.[59] It is important to note that the 4D fingerprint was generated using both the previously identified leads (active ligands) and inactive compounds (considered as decoys).[30] The multiple conformation states of each ligand in the database were generated using OMEGA (OpenEye Scientific Software).[60−62] Thereafter, we utilized the "docking option" of the SABRE program to place the filtered conformations of each ligand into the active site of the MycP$_1$ (PDB ID: 4HVL) and ranked them using the *HWK* scoring function.

Drug Repurposing Approach Using the 4D Finger-print. According to eq 14, the candidate B^i structure is similar to the set of known active ligands {A$_i$} if $V_{B^i}^* \in [min(V_{\{A^i\}}^*)$; $max(V_{\{A^i\}}^*)]$ and $V_{B^i}^* \approx V_A^{PHARM} \approx V_{AB}$, which results in *HWK* converging to 1. The volume V_A^{PHARM} is defined by the 4D fingerprint coefficients {C_k} that encoded the chemical features of the consensus molecular shape pattern of known active ligands (eq 7) for the specific binding target. Therefore, this suggests that the best fitted and most highly ranked ligands from the VS of the database have similar 4D fingerprint coefficients and thus should interact with the receptor of the known active ligands (concept of the drug-target profile). It is important to note that this approach considers only the 4D fingerprint and the fast-fitting method implemented in the SABRE program. To validate the effectiveness of SABRE for drug repurposing, we conducted a ligand- and structure-based VS procedure using the FDA database.

In Vitro Assay of MycP$_1$ Inhibitors. Recombinant *Mycobacterium thermoresistibile* MycP$_1$ was expressed and purified as reported previously.[43] A quenched, fluorescent peptide assay was used to measure the activity of MycP$_1$ in the presence of inhibitors. MycP$_1$ was used to digest 20 μM of the fluorescent substrate, AbzAVKAASLGK(Dnp)OH (GenScript Inc.). Potential MycP$_1$ inhibitors identified by SABRE were diluted to a concentration of 150 μM, and assays were measured in 96-well format. Compounds that were considered hits showed less than 50% activity compared to controls (DMSO-buffer blank). The same in vitro assay was used to measure the inhibitory concentration 50% (IC$_{50}$) of the most promising hits. For IC$_{50}$ measurements, inhibitors were added at 0, 5, 10, 50, 100, 200, 350, and 500 μM concentrations. Initial rates of fluorescent peptide hydrolysis were measured then incorporated into dose−response curves using GraphPad Prism.

■ RESULTS AND DISCUSSION

Performance of the SABRE^{HWK} Scoring Function. We evaluated the accuracy of the *HWK* scoring function and compared the current values to those obtained with the
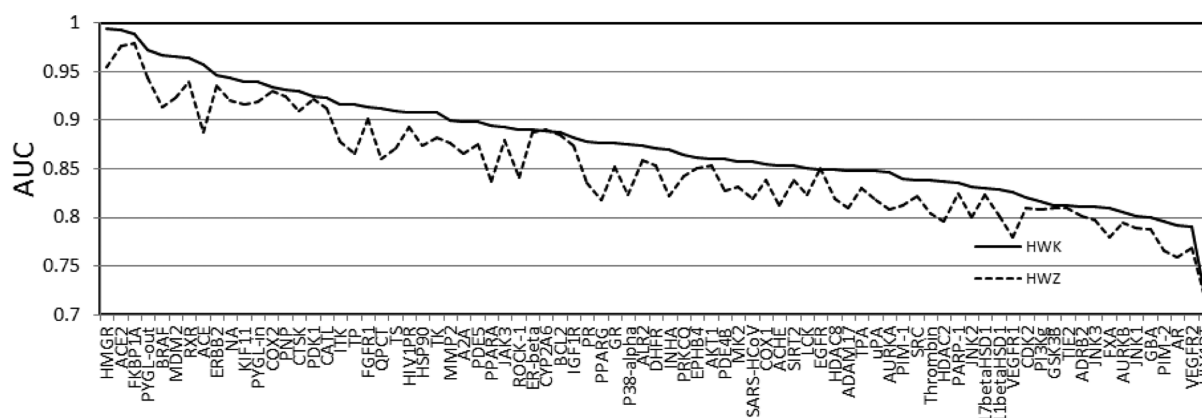
Figure 2. Comparison of the areas under the ROC curves (AUC) of the 81 DEKOIS databases using the SABRE^{HWK} and SABRE^{HWZ} scoring functions.
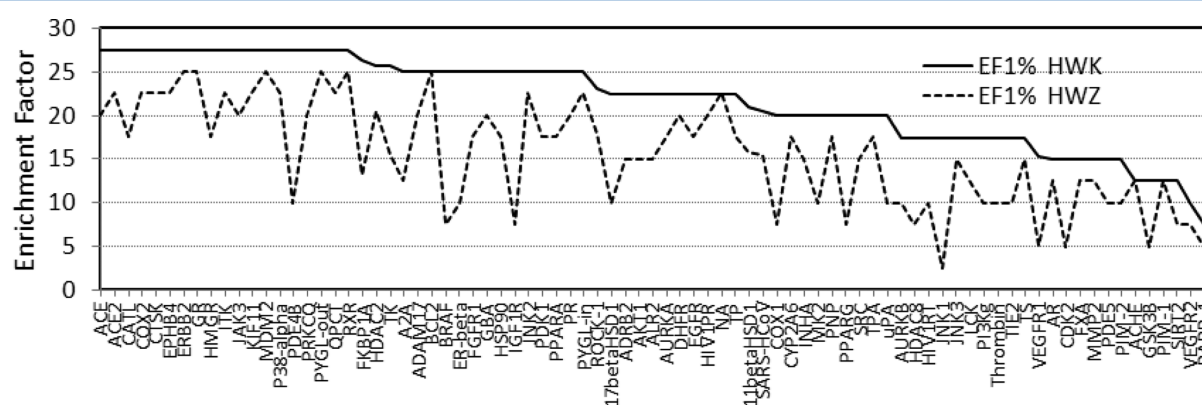

Figure 3. Comparison of the Enrichment Factor EF at 1% of the 81 DEKOIS databases using the SABRE^{HWK} and SABRE^{HWZ} scoring functions.

empirical *HWZ* scoring function[17] using the multi conformational states of the decoys and active ligands of the 81 targets from the DEKOIS database. The merits of scoring function became clear as it accurately ranked compounds with subtle structural changes. In the present VS trial, we selected query molecules according to the procedures presented in Kirchmair et al.[63] and used to describe the performance of the algorithms.[29,49]

As shown in Figure 2, we evaluated the AUC for each target of the DEKOIS database and the average AUC using the SABRE^{HWK} and SABRE^{HWZ} scoring functions. The average AUC value of the best performing query for the 81 DEKOIS targets using *HWK* and *HWZ* scoring functions was 0.875 ± 0.054 and 0.851 ± 0.054, respectively. The two scoring functions had similar overall performance for some of the 81 targets based on the AUC metric; however, an analysis of the complete set of targets revealed that SABRE^{HWK} performed more consistently in terms of AUC with an average AUC ≥ 0.9 for 26 targets and 0.9 > AUC ≥ 0.8 for 51 targets than SABRE^{HWZ}. Moreover, SABRE^{HWK} did not fail for any of the 81 targets screened. In comparison, SABRE^{HWZ} ranked the screening results with an AUC > 0.9 for only 17 of the 81 DEKOIS targets (11 targets out of 81 have AUC ≤ 0.8). The detailed results for each target are displayed in Table SI-1. One of the advantages of the SABRE^{HWK} approach is that the VS performance combining the 4D fingerprint and the novel *HWK* scoring function depended less on the screened targets, as already observed in our previous benchmark tests using the *HWZ* function with the 40 DUD targets.[17,18,29]

Analysis of the Enrichment Factor Using the SABRE^{HWK} Scoring Function. The efficiency of the SABRE^{HWK} scoring function was evaluated using the enrichment factor at 1% (EF$^{1\%}$), and the results were also compared to those using the SABRE^{HWZ} function (Figure 3 and Table SI-1). The average EF$^{1\%}$ values for the 81 targets using the novel *HWK* and empirical *HWZ* score-based virtual screening were 21.8 ± 5.0 and 15.5 ± 5.9, respectively. The SABRE^{HWK} method performed more consistently resulting in an EF$^{1\%}$ less than 10% for only two targets, whereas the results using the SABRE^{HWZ} method provided enrichment factors below 10% for 24 targets. Thus, the enrichments achieved with SABRE^{HWK} are considerably better than those obtained with the empirical *HWZ* scoring function, indicating that the novel scoring function was more efficient in identifying hits with notably different scaffolds compared to the query structure. Therefore, on the basis of the AUC and enrichment factor EF values, these results indicated that the novel *HWK* score demonstrated an improved and robust VS performance, albeit with the caveat that we used only 81 targets in this study.

Identification of Novel Inhibitors of MycP$_1$ Protease. The SABRE program was generally applicable for ranking any bioactive scaffold classes with the exception of inactive decoys. The recognition of a wide variety of structurally different ligand classes was an important goal of our virtual screening strategy. The MycP$_1$ protease represented a challenge for both ligand- and structure-based virtual-screening approaches. Indeed, only the crystal structure of the apo form of the enzyme was available, and the protein active site is relatively large, which

Table 1. Experimentally Determined Inhibitory Activity of the 13 Compounds Selected from the Virtual Screening

	compound	name	% inhibition at 150 μM	IC$_{50}$ (μM)[a]	PAINS filter[c]
NCI database	*1 (query)*	*NSC-357905*	*73.0%*	*48.0[b]*	*pass*
	2	NSC-67021	71.5%	76.8	pass
	3	NSC-270375	75.8%		pass
	4	NSC-67931	63.8%		pass
	5	NSC-356820	68.5%		fail
	6	NSC-206155	54.7%		pass
	7	NSC-614859	54.3%		pass
	8	NSC-207092	55.6%		fail
	9	NSC-111151	52.5%		fail
	10	NSC-641874	57.3%		pass
FDA database	11	Hydroxystilbamidine	79.1%	85.6	pass
	12	Diminazene	58.0%		fail
	13	Thiacetazone	80.1%		pass

[a]Only IC$_{50}$ < 100 μM are reported. [b]IC$_{50}$ value according to ref 30. [c]Pan Assay Interference Compounds (PAINS) remover, see ref 64.
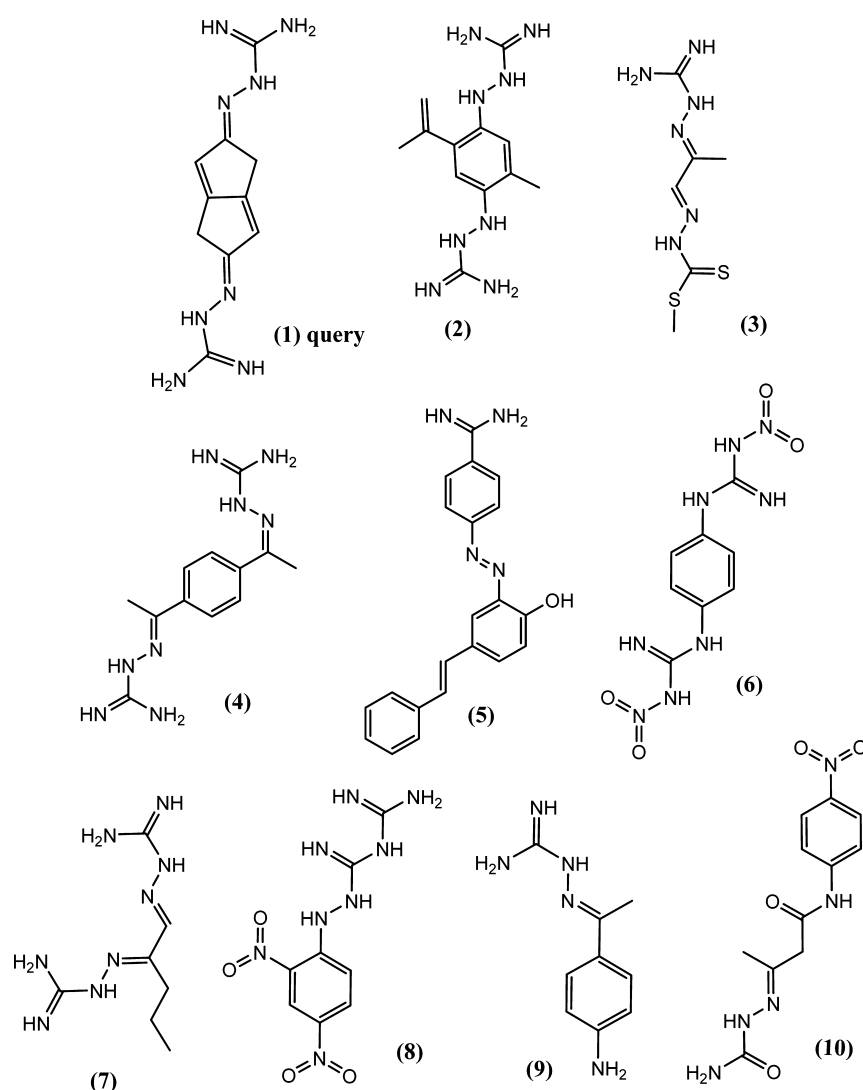
Figure 4. Structural scaffold of MycP$_1$ inhibitors identified during the VS of the NCI database.

decreased the probability of successfully identifying and ranking the correct pose of the screened ligands. The structures of MycP$_1$ inhibitors that we previously reported were available, and visual analysis of their putative poses in the active site revealed that the binding mode of compound **1** was reasonable.[30] These compounds have chemical features that

enabled SAR (structure−activity relationship) studies and generated a novel 4D fingerprint. For the purpose of SAR, an intuitive strategy for scaffold-hopping used the hit compound **1** as query and the HWK^+_{Dock} scoring function to rank hits with larger volume sizes from the NCI database. We constructed such a ranking of the best 1000 structures (top-1000) according
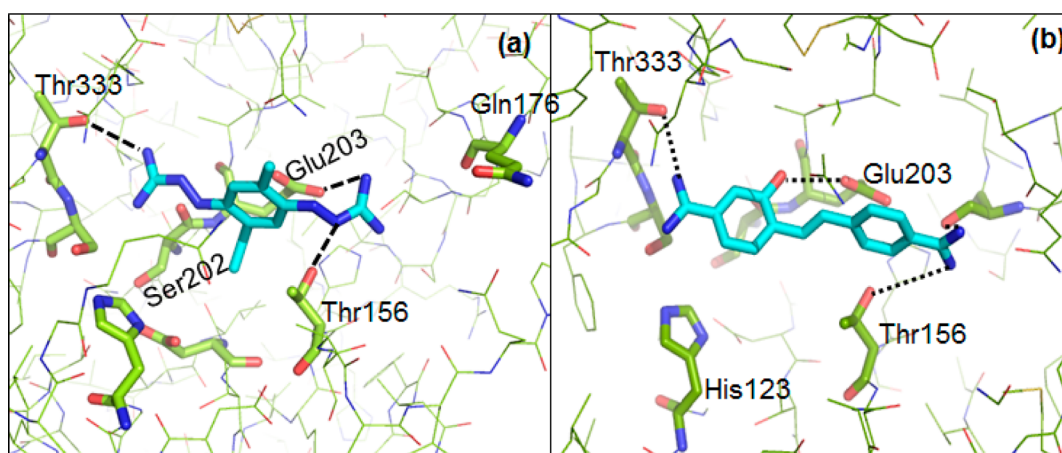
2840

dx.doi.org/10.1021/ci5003872 | *J. Chem. Inf. Model.* 2014, 54, 2834−2845

Figure 5. Stick view of the binding compound **2** (NSC-67021) and **11** (Hydroxystilbamidine) in the MycP$_1$ active site.

to the docking-score function. The pharmacophore model reduced the number of these structures to a small subset of promising MycP$_1$ lead candidates. The 135 hits derived from the NCI database were superimposed with the binding query (compound **1**) and visually inspected. Forty molecules were selected from the hits and tested in vitro for inhibitory activity against MycP$_1$. Notably, 9 compounds out of the 40 were able to inhibit MycP$_1$ by more than 50% when added at 150 μM (Table 1 and Figure 4) and one compound showed an IC$_{50}$ less than 100 μM. Compound **2** inhibited MycP$_1$ activity in the low micromolar range with an IC$_{50}$ of 76.8 μM and does not includes substructures described as Pan Assay Interference Compounds (PAINS).[64]

The VS procedure identified these compounds based on their common chemical features (4D fingerprint) present in the subset of known active ligand structures and their fit in the binding pocket. The coefficients of the 4D fingerprint efficiently encoded the spatial distributions of pharmacophoric points providing the alignment of compounds relative to the binding site surfaces. Each point accounted for an important chemical feature such as hydrogen bond donors/acceptors and negative/positive charged groups. The basic physicochemical features of the known MycP$_1$ compounds included the potential to establish hydrogen bonds as donors with Thr156 and Ser202, Glu203 and Thr333 residues. (Figure 5). Furthermore, analysis of the docking results revealed that the lead compound **2** fit well within the binding site cavity. The compound **2** formed hydrogen bonds with the Thr156, Thr333, Ser202, and Glu203 residues of MycP$_1$. The results were in agreement with our previous docking studies pointing out Ser202 and Thr156 as key residues to stabilize the ligand scaffold in the MycP$_1$ catalytic binding site.[30] A detailed analysis of the docking mode of the 11 compounds (Figure 4) revealed a close match between the pattern of hydrophobic and hydrogen bond donor pharmacophoric points of these hits compared to the pharmacophore model defined in our previous study.[30]

As shown in Table 2, the VS procedure ranked 9 lead compounds at different cut-offs among the initial 1000 docked structures. Among the top-30, one lead compound was present, and this outcome corresponded to 11% coverage. Furthermore, the 9 lead compounds were among the top-300 of the filtered NCI database. These results highlight the merits of our 4D fingerprint VS approach when combined with the novel HWK scoring function. We also compared this simple approach to a complex approach including other likely query conformations.

Table 2. Percent of Lead Compounds Recovered at Different Cutoffs of the Final Docked and Ranked Structures

cut off (top structures)	number of leads[a]	% coverage of leads[b]
30	1	11
75	4	44
150	5	55
300	9	100

[a]Total lead structures = 9. [b]% coverage of leads = (number of leads in the top/total lead) × 100.

We modeled three plausible binding poses of the compound **1** (query) with different conformations in MycP$_1$ cavity and redocked the top-1000 ligands using these three conformations, as shown in Table 2. The fusion approach markedly improved the percentage of retrieved lead compounds in the top-75 and further underscored the potential of the 4D fingerprint and HWK_{Dock} scoring VS procedure in the identification of lead compounds using the structure of unliganded receptor.

Assessment of the 4D Fingerprint and *HWK* Scoring Function for Drug Repurposing. The integration of this newly generated computational method, which combined the 4D fingerprint and the *HWK* scoring function with in vitro enzyme inhibition studies, was a useful approach for evaluating current drugs, already on the market for a particular therapeutic purpose as potential agents for treating TB. To demonstrate the applicability of this integrated virtual and experimental screening for drug-repurposing, we undertook the virtual screening of the FDA-approved drug database consisting of 1,217 compounds (corresponding to 3358 structures including tautomers) using the 4D fingerprints previously generated during NCI database screening. Hits were evaluated using the aforementioned MycP$_1$ enzyme assay. In order to increase the structural diversity of the compounds identified by this process, we conducted the VS procedure three times using compounds **1**, **8**, and **9** as query for each VS round. The choice of the structural query was critical to the success of this approach. As described in Methods, the scaffold diversity depended on the selected *HWK*$^-$ or *HWK*$^+$ or *HWK*^{T} (Tanimoto) scoring equations, which also depended on the query size. Thus, compound **1**, discovered in our previous work, was used as query since it has the highest affinity to MycP$_1$. The compounds **8** (larger volume than that of compound **1**) and **9** (smaller volume than that of compound **1**) were selected based on their differential volumes and structural diversity
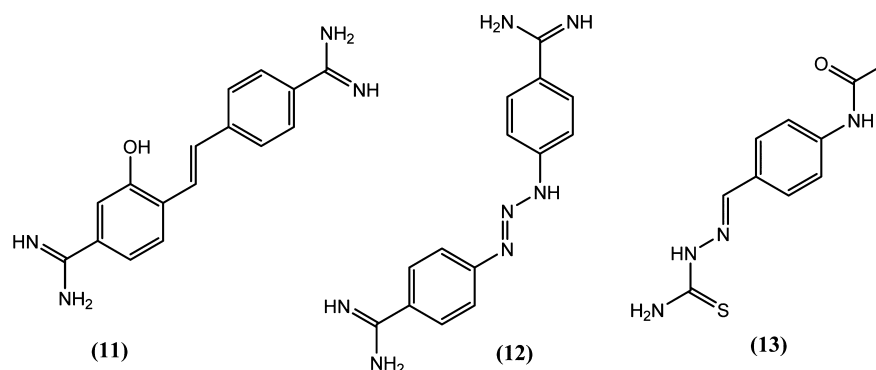
Figure 6. Structural scaffolds of MycP$_1$ inhibitors identified during the VS of the FDA database. The percentage of inhibition and IC$_{50}$ are displayed.

compared to the structure of **1**. The goal of our screen was to find hits with diverse structural scaffolds and comparable volume sizes to the queries. Thus, the resulting docked ligands of the FDA database were ranked using the $HWK_{Dock}^{Tanimoto}$ scoring function (eq 19).

Since the screening process of the NCI database and the benchmark test using the 4D fingerprint of SABRE program demonstrated high enrichment factor at 1% of the screened database, we visually inspected the binding mode of the best 30 structures (~1%) identified within the FDA database. We focused, in particular, on four compounds based on their high $HWK_{Dock}^{Tanimoto}$ docking score and their interactions with the key residues (Thr156 and Ser202) of the MycP1 binding cavity. These four compounds were chosen for in vitro inhibition assays, and three out of the four selected compounds exhibited more than 50% inhibition of MycP$_1$ when used at 150 μM (Table 1), which validated the merits of our VS approach. Finally, the active compounds were filtered for Pan Assay Interference Compounds (PAINS) (Table 1) and showed that the hydroxystilbamidine scaffold may be used as starting structure for further optimization. An analysis of the three ranked FDA approved drugs showed that the compounds **11**, **12**, and **13** were ranked by SABRE near the top at positions 2, 24, and 3 out of 1217. The high score for compounds **11** and **13** was attributable to the $HWK_{Dock}^{Tanimoto}$ scoring function, which took into account the ligand similarity as well as the optimal ligand/receptor pharmacophore model (eq 19). Out of the three, compound **11** had the greatest effect, with an IC$_{50}$ of 85.6 μM, whereas the two other leads had IC$_{50}$ > 100 μM. In addition, we noted the low structural similarity between the three identified FDA compounds (Figure 6). As observed for the other leads, compound **11** formed hydrogen bonds with the Thr156, Glu203, and Thr333 residues of the MycP$_1$ active site (Figure 5). Interestingly, compound **11** is typically used as a histochemical stain to understand the distribution and localization of biomarkers,[65] and these results suggested that it or its analogs may be repurposed for inhibition of MycP$_1$. More importantly, these preliminary findings show that the SABRE algorithm with HWK scoring provides an efficient means for the identification of new uses for current drugs and encourages us to pursue the applicability of methodology in drug repurposing strategy for other medically relevant drug targets.

Assessment of Lead Scaffold Diversity. Published data suggested counting hits only when the chemotype of a molecule is not equal to a template chemotype or any other chemotype that already exists in the hit list.[66] This approach resulted in a chemotype enrichment that emphasizes discovery

of ligands with different chemotype properties. We assessed the novelty of the confirmed 12 hits by comparing their structural similarities with a "simple 2D descriptor".[67] We computed the pairwise similarity index using the molecular access system MACCS structural keys (MACCS, 166 bits) of our 13 compounds (query +12 leads) and represented the structural diversity using the heat map (Figure 7). The MACCS similarity
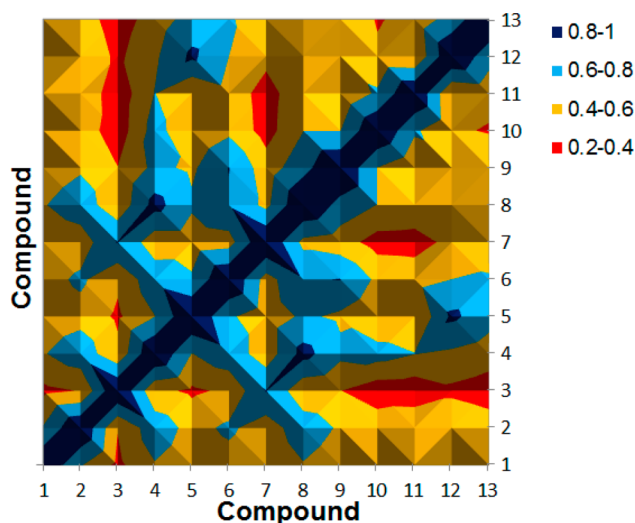

Figure 7. Heat map of the MACCS similarity index for the 13 compounds (12 leads + query).

indexes were calculated using Openbabel.[68] The map visualizes 15 × 15 = 225 pairwise comparisons and was color-coded by similarity values ranging from red (low similarity value) to dark blue (high similarity value). We observed only two lobes in dark blue consistent with high similarity between the compounds (MACCS index > 0.8) and most of the compounds were dissimilar. This result supported the increased structural diversity (MACCS index < 0.6) of the new lead compounds using the combined 4D fingerprint and HWK scoring function. Considering the high degree of substructure encoded in each VS round, it was not surprising that the 4D fingerprint algorithm performed well at finding diverse chemotypes.

■ CONCLUSION

We report a rational method for the design of novel scoring function HWK and validated its performance using a large number of targets from the DEKOIS database. The VS approach test using the 4D fingerprint and the HWK scoring

function provided high enrichment factors in detecting active compounds at early stage of the 81 screened databases. We validated the efficiency of the combined 4D fingerprint and *HWK* scoring function in scaffold-hopping strategy through the identification of nine novel lead compounds in a short hit list from the VS of the NCI database. The result of the VS round ranked these compounds in the top-300 of the database, and one of them displayed an IC_{50} comparable to that of the reference structure.

In the absence of new drugs for infectious diseases like TB, it made sense to develop a VS strategy capable of exploring databases of current drugs used to treat diseases other than infectious diseases and potentially repurpose some of them for TB treatment.[9−11] The merit of this approach lies in the obvious point that these commercially available drugs lack significant toxicity or side-effects.[12−14] To test this notion, the screening of the FDA database using our screening approach identified three FDA-approved compounds as potential lead structures. One of these compounds displayed an IC_{50} of 85.6 μM against $MycP_1$ protease. The distributions of pairwise structural similarities presented in the heat map revealed that the 13 lead compounds resulting from the VS of NCI and FDA databases were structurally diverse. In summary, this study represents the comprehensive quantification of VS approach for scaffold-hopping and drug repurposing and provides a solid strategy for the discovery of new classes of $MycP_1$ inhibitors.

ASSOCIATED CONTENT

Ⓢ Supporting Information

Detailed information about the enrichment factor at top 1% and the ROC (AUC) values for the 81 DEKOIS targets using SABRE program and rank of lead compounds from NCI and FDA databases. These information are available free of charge via the Internet at http://pubs.acs.org.

AUTHOR INFORMATION

Corresponding Author
*E-mail kkorotkov@uky.edu. Phone 859-323-5493. Fax 859-257-2283.

Present Address
#Department of Molecular Physiology and Biological Physics and The Myles H. Thaler Center for AIDS and Human Retrovirus Research, University of Virginia, Charlottesville, Virginia 22908, United States.

Notes
The authors declare no competing financial interest.

ACKNOWLEDGMENTS

REFERENCES

(1) Polgar, T.; Keseru, G. M. Integration of virtual and high throughput screening in lead discovery settings. *Comb. Chem. High Throughput Screen.* **2011**, *14*, 889−897.

(2) Langer, T.; Hoffmann, R. D. Virtual screening: an effective tool for lead structure discovery? *Curr. Pharm. Des.* **2001**, *7*, 509−527.

(3) John, S.; Thangapandian, S.; Sakkiah, S.; Lee, K. W. Discovery of potential pancreatic cholesterol esterase inhibitors using pharmacophore modelling, virtual screening, and optimization studies. *J. Enzyme Inhib. Med. Chem.* **2011**, *26*, 535−545.

(4) Bi, J.; Yang, H.; Yan, H.; Song, R.; Fan, J. Knowledge-based virtual screening of HLA-A*0201-restricted CD8(+) T-cell epitope peptides from herpes simplex virus genome. *J. Theor. Biol.* **2011**, *281*, 133−139.

(5) Akula, N.; Zheng, H.; Han, F. Q.; Wang, N. Discovery of novel SecA inhibitors of *Candidatus* Liberibacter asiaticus by structure based design. *Bioorg. Med. Chem. Lett.* **2011**, *21*, 4183−4188.

(6) Englebienne, P.; Moitessier, N. Docking ligands into flexible and solvated macromolecules. 4. Are popular scoring functions accurate for this class of proteins? *J. Chem. Inf. Model.* **2009**, *49*, 1568−1580.

(7) Bleicher, K. H.; Green, L. G.; Martin, R. E.; Rogers-Evans, M. Ligand identification for G-protein-coupled receptors: a lead generation perspective. *Curr. Opin. Chem. Biol.* **2004**, *8*, 287−296.

(8) Gohlke, H.; Klebe, G. Approaches to the description and prediction of the binding affinity of small-molecule ligands to macromolecular receptors. *Angew. Chem., Int. Ed. Engl.* **2002**, *41*, 2645−2676.

(9) Boguski, M. S.; Mandl, K. D.; Sukhatme, V. P. Repurposing with a difference. *Science* **2009**, *324*, 1394−1395.

(10) D'Oca, G. Program aims to find new use for old drugs. *Future Med. Chem.* **2013**, *5*, 1372−1372.

(11) Conticello, C.; Martinetti, D.; Adamo, L.; Buccheri, S.; Giuffrida, R.; Parrinello, N.; Lombardo, L.; Anastasi, G.; Amato, G.; Cavalli, M.; Chiarenza, A.; De Maria, R.; Giustolisi, R.; Gulisano, M.; Di Raimondo, F. Disulfiram, an old drug with new potential therapeutic uses for human hematological malignancies. *Int. J. Cancer* **2012**, *131*, 2197−2203.

(12) Gleeson, M. P.; Hersey, A.; Montanari, D.; Overington, J. Probing the links between in vitro potency, ADMET and physicochemical parameters. *Nat. Rev. Drug Discovery* **2011**, *10*, 197−208.

(13) MacDonald, M. L.; Lamerdin, J.; Owens, S.; Keon, B. H.; Bilter, G. K.; Shang, Z.; Huang, Z.; Yu, H.; Dias, J.; Minami, T.; Michnick, S. W.; Westwick, J. K. Identifying off-target effects and hidden phenotypes of drugs in human cells. *Nat. Chem. Biol.* **2006**, *2*, 329−337.

(14) Bender, A.; Scheiber, J.; Glick, M.; Davies, J. W.; Azzaoui, K.; Hamon, J.; Urban, L.; Whitebread, S.; Jenkins, J. L. Analysis of pharmacology data and the prediction of adverse drug reactions and off-target effects from chemical structure. *ChemMedChem.* **2007**, *2*, 861−873.

(15) Venkatraman, V.; Perez-Nueno, V. I.; Mavridis, L.; Ritchie, D. W. Comprehensive comparison of ligand-based virtual screening tools against the DUD data set reveals limitations of current 3D methods. *J. Chem. Inf. Model.* **2010**, *50*, 2079−2093.

(16) Giganti, D.; Guillemain, H.; Spadoni, J.-L.; Nilges, M.; Zagury, J.-F.; Montes, M. Comparative evaluation of 3D virtual ligand screening methods: impact of the molecular alignment on enrichment. *J. Chem. Inf. Model.* **2010**, *50*, 992−1004.

(17) Hamza, A.; Wei, N. N.; Zhan, C. G. Ligand-based virtual screening approach using a new scoring function. *J. Chem. Inf. Model.* **2012**, *52*, 963−974.

(18) Hamza, A.; Wei, N.-N.; Hao, C.; Xiu, Z.; Zhan, C.-G. A novel and efficient ligand-based virtual screening approach using the HWZ scoring function and an enhanced shape-density model. *J. Biomol. Struct. Dyn.* **2012**, *31*, 1236−1250.

(19) Hert, J.; Willett, P.; Wilton, D. J.; Acklin, P.; Azzaoui, K.; Jacoby, E.; Schuffenhauer, A. New methods for ligand-based virtual screening: use of data fusion and machine learning to enhance the effectiveness of similarity searching. *J. Chem. Inf. Model.* **2006**, *46*, 462−470.

(20) Wang, R. X.; Wang, S. M. How does consensus scoring work for virtual library screening? An idealized computer experiment. *J. Chem. Inf. Comput. Sci.* **2001**, *41*, 1422−1426.

(21) Charifson, P. S.; Corkery, J. J.; Murcko, M. A.; Walters, W. P. Consensus scoring: a method for obtaining improved hit rates from docking databases of three-dimensional structures into proteins. *J. Med. Chem.* **1999**, *42*, 5100−5109.

(22) Hert, J.; Willett, P.; Wilton, D. J. Comparison of fingerprint-based methods for virtual screening using multiple bioactive reference structures. *J. Chem. Inf. Comput. Sci.* **2004**, *44*, 1177−1185.

(23) Hopfinger, A. J.; Wang, S.; Tokarski, J. S.; Jin, B. Q.; Albuquerque, M.; Madhav, P. J.; Duraiswami, C. Construction of 3D-QSAR models using the 4D-QSAR analysis formalism. *J. Am. Chem. Soc.* **1997**, *119*, 10509−10524.

(24) Pan, D. H.; Iyer, M.; Liu, J. Z.; Li, Y.; Hopfinger, A. J. Constructing optimum blood brain barrier QSAR models using a combination of 4D-molecular similarity measures and cluster analysis. *J. Chem. Inf. Comput. Sci.* **2004**, *44*, 2083−2098.

(25) Senese, C. L.; Duca, J.; Pan, D.; Hopfinger, A. J.; Tseng, Y. J. 4D-fingerprints, universal QSAR and QSPR descriptors. *J. Chem. Inf. Comput. Sci.* **2004**, *44*, 1526−1539.

(26) Iyer, M.; Hopfinger, A. J. Treating chemical diversity in QSAR analysis: modeling diverse HIV-1 integrase inhibitors using 4D fingerprints. *J. Chem. Inf. Model.* **2007**, *47*, 1945−1960.

(27) Pasqualoto, K. F. M.; Ferreira, E. I.; Santos, O. A.; Hopfinger, A. J. Rational design of new antituberculosis agents: receptor-independent four-dimensional quantitative structure-activity relationship analysis of a set of isoniazid derivatives. *J. Med. Chem.* **2004**, *47*, 3755−3764.

(28) Andrade, C. H.; Pasqualoto, K. F. M.; Ferreira, E. I.; Hopfinger, A. J. 4D-QSAR: perspectives in drug design. *Molecules* **2010**, *15*, 3281−3294.

(29) Wei, N.-N.; Hamza, A. SABRE: Ligand/structure-based virtual screening approach using consensus molecular-shape pattern recognition. *J. Chem. Inf. Model.* **2014**, *54*, 338−346.

(30) Hamza, A.; Wagner, J. M.; Evans, T. J.; Frasinyuk, M. S.; Kwiatkowski, S.; Zhan, C.-G.; Watt, D. S.; Korotkov, K. V. Novel mycosin protease MycP1 inhibitors identified by virtual screening and 4D fingerprints. *J. Chem. Inf. Model.* **2014**, *54*, 1166−1173.

(31) WorldHealthOrganization. WHO global tuberculosis report. 2013, http://www.who.int/tb/publications/global_report/en/ (accessed on July 2, 2014).

(32) Payne, D. J.; Gwynn, M. N.; Holmes, D. J.; Pompliano, D. L. Drugs for bad bugs: confronting the challenges of antibacterial discovery. *Nat. Rev. Drug Discovery* **2007**, *6*, 29−40.

(33) Fischbach, M. A.; Walsh, C. T. Antibiotics for emerging pathogens. *Science* **2009**, *325*, 1089−1093.

(34) Chen, J. M.; Pojer, F.; Blasco, B.; Cole, S. T. Towards anti-virulence drugs targeting ESX-1 mediated pathogenesis of *Mycobacterium tuberculosis*. *Drug Discovery Today Dis. Mech.* **2010**, *7*, e25−e31.

(35) Bottai, D.; Serafini, A.; Cascioferro, A.; Brosch, R.; Manganelli, R. Targeting type VII/ESX secretion systems for development of novel antimycobacterial drugs. *Curr. Pharm. Des.* **2014**, *20*, 4346−4356.

(36) Stanley, S. A.; Raghavan, S.; Hwang, W. W.; Cox, J. S. Acute infection and macrophage subversion by *Mycobacterium tuberculosis* require a specialized secretion system. *Proc. Natl. Acad. Sci. U.S.A.* **2003**, *100*, 13001−13006.

(37) Stoop, E. J. M.; Bitter, W.; van der Sar, A. M. Tubercle bacilli rely on a type VII army for pathogenicity. *Trends Microbiol.* **2012**, *20*, 477−484.

(38) Houben, E. N.; Korotkov, K. V.; Bitter, W. Take five — type VII secretion systems of *Mycobacteria*. *Biochim. Biophys. Acta* **2014**, *1844*, 1707−1716.

(39) McLaughlin, B.; Chon, J. S.; MacGurn, J. A.; Carlsson, F.; Cheng, T. L.; Cox, J. S.; Brown, E. J. A *Mycobacterium* ESX-1-secreted virulence factor with unique requirements for export. *PLoS Pathog.* **2007**, *3*, 1051−1061.

(40) Xu, J.; Laine, O.; Masciocchi, M.; Manoranjan, J.; Smith, J.; Du, S. J.; Edwards, N.; Zhu, X.; Fenselau, C.; Gao, L.-Y. A unique *Mycobacterium* ESX-1 protein co-secretes with CFP-10/ESAT-6 and is necessary for inhibiting phagosome maturation. *Mol. Microbiol.* **2007**, *66*, 787−800.

(41) Chen, J. M.; Zhang, M.; Rybniker, J.; Boy-Röttger, S.; Dhar, N.; Pojer, F.; Cole, S. T. *Mycobacterium tuberculosis* EspB binds phospholipids and mediates EsxA-independent virulence. *Mol. Microbiol.* **2013**, *89*, 1154−1166.

(42) Ohol, Y. M.; Goetz, D. H.; Chan, K.; Shiloh, M. U.; Craik, C. S.; Cox, J. S. *Mycobacterium tuberculosis* MycP1 protease plays a dual role in regulation of ESX-1 secretion and virulence. *Cell Host Microbe* **2010**, *7*, 210−220.

(43) Wagner, J. M.; Evans, T. J.; Chen, J.; Zhu, H.; Houben, E. N.; Bitter, W.; Korotkov, K. V. Understanding specificity of the mycosin proteases in ESX/type VII secretion by structural and functional analysis. *J. Struct. Biol.* **2013**, *184*, 115−128.

(44) Solomonson, M.; Huesgen, P. F.; Wasney, G. A.; Watanabe, N.; Gruninger, R. J.; Prehna, G.; Overall, C. M.; Strynadka, N. C. Structure of the mycosin-1 protease from the mycobacterial ESX-1 protein type VII secretion system. *J. Biol. Chem.* **2013**, *288*, 17782−17790.

(45) Sun, D.; Liu, Q.; He, Y.; Wang, C.; Wu, F.; Tian, C.; Zang, J. The putative propeptide of MycP1 in mycobacterial type VII secretion system does not inhibit protease activity but improves protein stability. *Protein Cell* **2013**, *4*, 921−931.

(46) Bauer, M. R.; Ibrahim, T. M.; Vogel, S. M.; Boeckler, F. M. Evaluation and optimization of virtual screening workflows with DEKOIS 2.0 — a public library of challenging docking benchmark sets. *J. Chem. Inf. Model.* **2013**, *53*, 1447−1462.

(47) Mavridis, L.; Hudson, B. D.; Ritchie, D. W. Toward high throughput 3D virtual screening using spherical harmonic surface representations. *J. Chem. Inf. Model.* **2007**, *47*, 1787−1796.

(48) Dror, O.; Schneidman-Duhovny, D.; Inbar, Y.; Nussinov, R.; Wolfson, H. J. Novel approach for efficient pharmacophore-based virtual screening: method and applications. *J. Chem. Inf. Model.* **2009**, *49*, 2333−2343.

(49) Yan, X.; Li, J.; Liu, Z.; Zheng, M.; Ge, H.; Xu, J. Enhancing molecular shape comparison by weighted Gaussian functions. *J. Chem. Inf. Model.* **2013**, *53*, 1967−1978.

(50) Mezey, P. G. Topological shape analysis of chain molecules: an application of the GSTE principle. *J. Math. Chem.* **1993**, *12*, 365−373.

(51) Walker, P. D.; Arteca, G. A.; Mezey, P. G. A complete shape characterization for molecular charge densities represented by Gaussian-type functions. *J. Comput. Chem.* **1991**, *12*, 220−230.

(52) Grant, J. A.; Pickup, B. T. A Gaussian description of molecular shape. *J. Phys. Chem.* **1995**, *99*, 3503−3510.

(53) Grant, J. A.; Gallardo, M. A.; Pickup, B. T. A fast method of molecular shape comparison: a simple application of a Gaussian description of molecular shape. *J. Comput. Chem.* **1996**, *17*, 1653−1666.

(54) Grant, J. A.; Pickup, B. T. A Gaussian description of molecular shape. *J. Phys. Chem.* **1996**, *100*, 2456−2456.

(55) Rogers, D. J.; Tanimoto, T. T. A computer program for classifying plants. *Science* **1960**, *132*, 1115−1118.

(56) Jacobsson, M.; Liden, P.; Stjernschantz, E.; Bostrom, H.; Norinder, U. Improving structure-based virtual screening by multi-variate analysis of scoring data. *J. Med. Chem.* **2003**, *46*, 5781−5789.

(57) Hecker, E. A.; Duraiswami, C.; Andrea, T. A.; Diller, D. J. Use of catalyst pharmacophore models for screening of large combinatorial libraries. *J. Chem. Inf. Comput. Sci.* **2002**, *42*, 1204−1211.

(58) Diller, D. J.; Li, R. X. Kinases, homology models, and high throughput docking. *J. Med. Chem.* **2003**, *46*, 4638−4647.

(59) Irwin, J. J.; Shoichet, B. K. ZINC — A free database of commercially available compounds for virtual screening. *J. Chem. Inf. Model.* **2005**, *45*, 177−182.

(60) OMEGA, version 2.5.1; OpenEye Scientific Software; Santa Fe, NM; http://www.eyesopen.com.

(61) Hawkins, P. C. D.; Skillman, A. G.; Warren, G. L.; Ellingson, B. A.; Stahl, M. T. Conformer generation with OMEGA: algorithm and validation using high quality structures from the Protein Databank and Cambridge Structural Database. *J. Chem. Inf. Model.* **2010**, *50*, 572−584.

(62) Hawkins, P. C. D.; Nicholls, A. Conformer generation with OMEGA: learning from the data set and the analysis of failures. *J. Chem. Inf. Model.* **2012**, *52*, 2919−2936.

(63) Kirchmair, J.; Distinto, S.; Markt, P.; Schuster, D.; Spitzer, G. M.; Liedl, K. R.; Wolber, G. How to optimize shape-based virtual screening: choosing the right query and including chemical information. *J. Chem. Inf. Model.* **2009**, *49*, 678−692.

(64) Baell, J. B.; Holloway, G. A. New substructure filters for removal of Pan Assay Interference Compounds (PAINS) from screening libraries and for their exclusion in bioassays. *J. Med. Chem.* **2010**, *53*, 2719−2740.

(65) Schmued, L. C.; Fallon, J. H. Fluoro-gold: a new fluorescent retrograde axonal tracer with numerous unique properties. *Brain Res.* **1986**, *377*, 147−154.

(66) Good, A. C.; Hermsmeier, M. A.; Hindle, S. A. Measuring CAMD technique performance: A virtual screening case study in the design of validation experiments. *J. Comput. Aided Mol. Des.* **2004**, *18*, 529−536.

(67) Jain, A. N.; Nicholls, A. Recommendations for evaluation of computational methods. *J. Comput. Aided Mol. Des.* **2008**, *22*, 133−139.

(68) O'Boyle, N. M.; Banck, M.; James, C. A.; Morley, C.; Vandermeersch, T.; Hutchison, G. R. Open Babel: an open chemical toolbox. *J. Cheminform.* **2011**, *3*, 33.

2845

dx.doi.org/10.1021/ci5003872 | *J. Chem. Inf. Model.* 2014, 54, 2834−2845